Article

Magnetic Hyperthermia and Antibacterial Response of CuCo₂O₄ Nanoparticles Synthesized through Laser Ablation of Bulk Alloy

Imran Ali [1], Yasir Jamil [2], Saeed Ahmed Khan [3], Yunxiang Pan [1], Aqeel Ahmed Shah [4], Ali Dad Chandio [4], Sadaf Jamal Gilani [5], May Nasser Bin Jumah [6,7,8], Yusra Fazal [1], Jun Chen [9,*] and Zhonghua Shen [1,*]

1   School of Science, Nanjing University of Science and Technology, Nanjing 210094, China
2   Laser Spectroscopy Lab, Department of Physics, University of Agriculture, Faisalabad 38040, Pakistan
3   Department of Electrical Engineering, Sukkur IBA University, Sukkur 65200, Pakistan
4   Wet Chemistry Laboratory, Department of Metallurgical Engineering, NED University of Engineering and Technology, Karachi 75270, Pakistan
5   Department of Basic Health Sciences, Foundation Year for the Health Colleges, Princess Nourah bint Abdulrahman University, Riyadh 11671, Saudi Arabia
6   Biology Department, College of Science, Princess Nourah bint Abdulrahman University, Riyadh 11671, Saudi Arabia
7   Environment and Biomaterial Unit, Health Sciences Research Center, Princess Nourah bint Abdulrahman University, Riyadh 11671, Saudi Arabia
8   Saudi Society for Applied Science, Princess Nourah bint Abdulrahman University, Riyadh 11671, Saudi Arabia
9   Institute of Optoelectronics & Nanomaterials, MIIT Key Laboratory of Advanced Display Materials and Devices, College of Materials Science and Engineering, Nanjing University of Science and Technology, Nanjing 210094, China
*   Correspondence: chenjun@njust.edu.cn (J.C.); shenzh@njust.edu.cn (Z.S.)

Abstract: The wide variety of uses for nanoparticles (NPs) is due to their unique combination of features in a single assembly. The arc melted copper-cobalt ingot sample were qualitatively studied using laser induced breakdown spectroscopy (LIBS). Later, using the fabricated alloy as a target material for Nd:YAG laser ablation, CuCo₂O₄ NPs were synthesized. The magnetic properties of the synthesized NPs were studied using a vibrating sample magnetometer (VSM). To determine the composition and morphology of the synthesized NPs, X-ray diffraction (XRD), energy dispersive X-ray (EDX) analysis, transmission electron microscopy (TEM), scanning electron microscopy (SEM), and dynamic light scattering (DLS) techniques were used. The TEM and DLS showed that particles were spherical in shape with an average size of 32 nm and 28 nm, respectively. The antibacterial activity of the synthesized NPs was studied against *S. aureus* and *E. coli* strains as positive and negative controls using a standard approach. CuCo₂O₄ nanoparticles exhibited non-mutagenic potential against *S. typhimurium TA-98* and *TA-100* strains. Furthermore, the magnetic hyperthermia study of CuCo₂O₄ nanofluid was examined using a lab-made apparatus. The specific absorption rates (SAR) of 4.57 and 5.17 W/g were determined for the magnetic field strength of 230 μT and 247 μT, respectively. The study shows antibacterial activity and magnetic hyperthermia potential of the synthesized nanoparticles.

Keywords: bimetallic nanoparticles; laser ablation; LIBS; antibacterial activity; Ames; magnetic hyperthermia

1. Introduction

Nanoparticles have a wide range of applications, including gas detection (such as methane) [1], photocatalysis [2], and high-performance supercapacitors [3], as well as in biological fields, notably for hyperthermia [4]. The use of temperature that is much higher than normal in the treatment of cancer is known as hyperthermia [5]. Many techniques, including Ohmic heating [6], whole-body hyperthermia [7], and microwave systems [8] have

been used to create hyperthermia temperature for treating cancer. One issue with these methods is how to regulate the temperature to the targeted diseased area [9,10]. The best hyperthermia delivery system would be tissue-specific, noninvasive, and able to heat deep tissues with precise localization and high intensity. In the 1950s, Gilchrist was the first to suggest using magnetic materials for inducing hyperthermia. Since then, magnetic nanoparticles have been proven to be capable of achieving each of these conditions [11]. Numerous drug delivery methods may be used to distribute magnetic nanoparticles non-invasively in stable colloidal solutions. They can be remotely heated after delivery using alternating magnetic fields at frequencies that do not harm healthy tissues. This provides effective deep tissue heating with small energy delivery pathways. The majority of the magnetic particles used in hyperthermia research are made of magnetite and similar spinels with nickel, cobalt, or other replacements [12]. Magnetic hyperthermia involves heating cancerous tissue to 41–46 °C by exposing magnetic nanoparticles to an alternating magnetic field (AMF) [13,14]. AMF produced hyperthermia using magnetic nanoparticles may have the advantage of targeting the heating of cancer tissue with low collateral harm [15,16]. The Neel relaxation and Brownian relaxation of particles in the presence of external magnetic fields contribute to the generation of heat in magnetic fluid hyperthermia [17]. Particles made of cobalt ferrite have a high level of magnetization saturation in addition to a high level of heating efficiency. Heating efficiencies may go much higher in the future since techniques for controlling these particles' size composition, shape, and size have not yet been completely developed as they have for iron oxides [18]. The sol-gel synthesis of cobalt-copper ferrite nanoparticles was investigated for their potential to induce magnetic hyperthermia [19]. The optimum temperature was achieved using copper-substituted $CoFe_2O_4$ nanoparticles coated with chitosan for magnetic fluid hyperthermia [20]. Aqueously dispersed $CoFe_2O_4$ nanoparticles have been reported to produce heat as heating mediators for magnetically driven drug delivery and magnetic hyperthermia [21]. $CuFe_2O_4$ nanoparticles were made using the solvothermal method for use in magnetic hyperthermia [22]. Cobalt-copper ferrite bioactive glass composites have been demonstrated in other studies to be effective materials for bone hyperthermia applications [23]. $CuCo_2O_4/CuO$ nanoparticles were studied for their anti-cancer properties, and cytotoxic effects against malignant cells [24]. There have also been reports of the synthesis of magnetic nanoparticles utilizing the laser ablation approach for magnetic hyperthermia application [25]. Recently, copper-iron and copper-nickel NPs were synthesized through laser ablation in water for antibacterial activities and magnetic hyperthermia studies [26]. Notably, studies have indicated that bacteria, such as *E.coli* (Gram-negative) and *S.aures* (Gram-positive), which have been found on the surface of mobile phones and display screens, may cause septicemia, dermatitis, and pneumonia [27,28]. Isopropyl alcohol cleaning of the surface of the displays is an important step in removing harmful germs and fungus. However, this method does not provide permanent antibacterial action [29]. It has been shown that diffusing nanoparticles or nanoclusters onto the surface of glass may provide outcomes with significant antibacterial property and durability [30]. Cobalt-copper ferrite particles with aluminum substitution have been discovered to have increased antibacterial activity [31]. In testing against different bacterial strains, the antibacterial properties of Au-doped glass were shown to be significantly improved [32]. Sol-gel [33], chemical precipitation [34], hydrothermal [35], solvothermal [36], and thermal decomposition/combustion [37] synthesis techniques have all been used to create nanoparticles. These synthesis techniques may have complications despite their advancements. These complications may include the requirement for multiple purification steps, lengthy and convoluted pathways, and contaminations [38]. The following benefits have made the laser ablation technique a successful method for synthesizing nanoparticles. In contrast to chemical techniques, the laser ablation method generates very pure nanoparticles that may be used directly in the fields of chemical, biological, medical, and biochemical research [39]. With the appropriate laser ablation parameters, almost all materials, including metals, polymeric and dielectrics materials, may be used to synthesize nanoparticles according to requirements. Even complex alloy or

multi-element nanoparticles are easily synthesized. Synthesis of nanoparticles is possible in the majority of the available solutions. It has a potential to generate particles with a wide range of characteristics, the process can be carried out in ambient atmosphere and at ambient temperature [39]. It is very effective, sustainable, only needs one step of synthesis, and is ecologically benign [40]. Pyrophoric, risky, or poisonous chemical precursors are not necessary. The substrate material in the laser ablation technique are often much less expensive than the compounds employed in chemical procedures. Additionally, there are no significant safety concerns [39]. One may find a complete overview [41] on the laser ablation of nanoparticles and the potential uses of these particles, and a summary of the literature on the growth of laser-ablated particles in liquids may be found in the review [42]. Precise size selection or control in various environments would be a crucial problem since direct laser ablation may produce a wide range of size distributions. During the process of laser ablation, the synthesis of nanoparticles can only take place in a small zone around the laser focus point. As a result, there was a decrease in the amount of nanoparticles synthesized by laser ablation [39]. Despite the fact that laser-assisted $CuCo_2O_4$ NPs are completely free of contaminants, very little study has been carried out on their usage for magnetic hyperthermia.

In this study, Cu and Co ingot was made through the arc melting process, and its composition was validated via the LIBS technique. Using a pulsed Nd:YAG 1064 nm laser, $CuCo_2O_4$ nanoparticles were produced. X-ray diffraction (XRD), scanning electron microscopy (SEM), energy dispersive X-ray (EDX), transmission electron microscopy (TEM), and dynamic light scattering (DLS) techniques were used to characterize the laser-assisted produced nanoparticles. The sample's magnetic characteristics were measured using a VSM (vibrating sample magnetometer). The Ames test and antibacterial activity were conducted to examine the biological characteristics of the generated nanomaterials. The magnetic hyperthermia of $CuCo_2O_4$ NPs was then studied using a lab-built hyperthermia equipment.

2. Materials and Methods

Using the described method [43], a bulk alloy of Cu and Co was synthesized by the arc melting technique (samples purchased at a purity of 99.99% from ZhongNuo Advanced Materials Beijing, Beijing, China, available at https://www.enfsolar.com/znxc-tech (accessed on 26 March 2019). Here, we briefly describe the experimental setup of laser-induced breakdown spectroscopy (LIBS) (Laser is Quantel Q Smart (Paris, France), Spectrometer is Avantes (Apeldoorn, The Netherlands) and Delay Generator is SRS545 Sunnyvale, CA, USA), which was used for the qualitative analysis of the fabricated bulk ingot. A Nd:YAG pulsed laser (Q-smart 850, 532 nm), a sample holder, a delay generator, a four-channel avantes spectrometer, and avantes software are some of the parts of the commercial LIBS system. The Nd:YAG pulsed laser used in this study had a repetition rate of 10 Hz and an energy of 190 mJ. Using a convex lens with a 12 cm focal length, the laser's beam was focused onto the ingot surface. The experiment used an optical multichannel analyzer with CCD pixels that could measure wavelengths from 190 nm to 770 nm with a resolution of 0.04 nm. Figure 1 depicts a LIBS configuration. For the synthesis of $CuCo_2O_4$ nanomaterials, a Nd:YAG pulsed laser beam (Q-smart 850, 6 ns, 1064 nm, 10 kHz, 190 mJ) was used. A lens with a focal length of 50 cm was used to focus the laser beam on the surface of an alloy target that was immersed in 15 ml of water solution and a schematic diagram is presented in Figure 2. Once mechanically polished and cleaned with deionized water, the bulk alloy target was placed in an ultrasonic tank for 15 min for washing before undergoing the synthesis process. The sample was ablated for 10 min, without being rotated, and the synthesis process using the identical production settings was repeated. An antibacterial response and Ames test were conducted to examine the biological activities of the synthesized NPs using standard procedures. The magnetic characteristics of the dried produced NPs were measured using a vibrating sample magnetometer (VSM; Lakeshore Model 7304, Westerville, OH, USA). For the study of compositions, shape, and size of the synthesized nanoparticles, X-ray diffraction (XRD; Miniflex 600; Rigaku; Austin, TX, USA),

energy dispersive X-ray (EDX), scanning electron microscopy (FEI Nova 450 NanoSEM, Thermofisher Scientific, Waltham, MA, USA) and transmission electron microscopy (JEM-2100F, JEOL, Tokyo, Japan) were employed to analyze the compositions, shapes, and sizes of the produced nanoparticles. A lab-made setup was used to study the magnetic hyperthermia of the synthesized nanofluid. An infrared thermometer (MLX90614, Melexis, Ypres, Belgium) was used for non-contact temperature measurements.
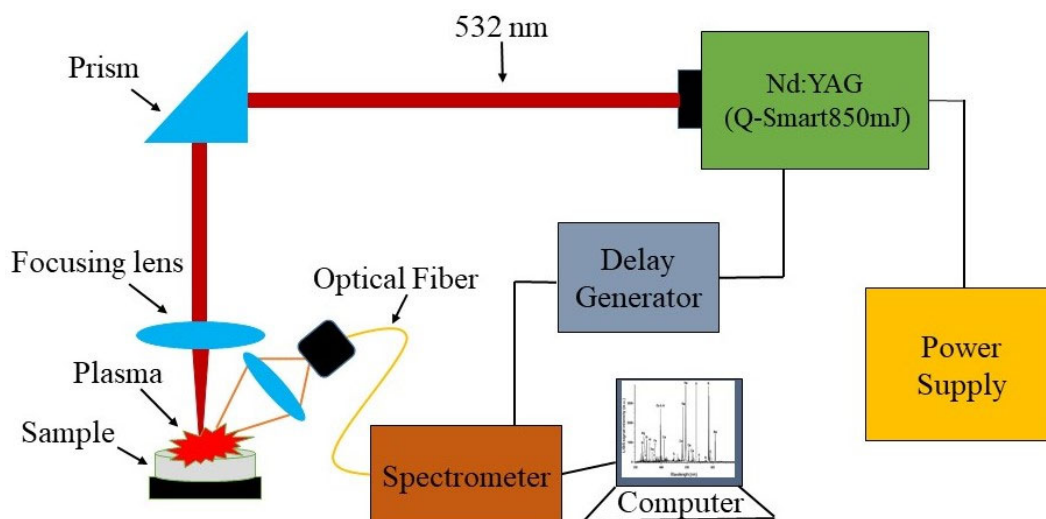

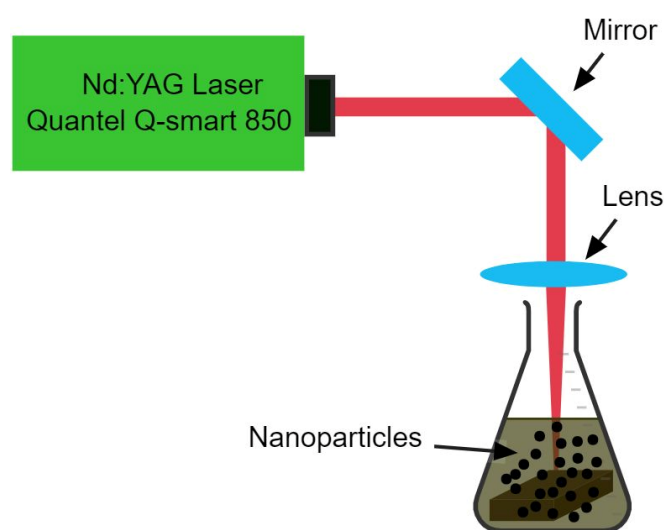**Figure 1.** Schematic diagram of the laser induced breakdown spectroscopy apparatus.

Figure 2. Laser ablation system for the generation of $CuCo_2O_4$ nanoparticles.

Proposed Synthesis Mechanism of NPs

The plasma generated by the higher intensity laser beam on the surface of the targeted sample induces solvent molecule disintegration, ionization, and atomization, resulting in nanoparticle synthesis utilizing pulsed laser ablation in water. During the process of rapidly quenching the plasma, the energy is transferred from the plasma to the water and may cause bubbles to develop in the solution. Emitted material fragments have the ability to participate in electrochemical reactions with reactive specimens generated from the target sample and disintegrated liquid molecules when the plasma is being formed and then quenched. The high collision rate generated by the high temperature and pressure turns species into particles. Due to expansion and compression, the cavitation bubbles collapsed at their threshold volume, releasing particles into the liquid. These ligand-free reactive nanomaterials have the ability to develop a wide range of unique nanomaterials

with a number of various geometries [44–47]. Irradiating a solution that already contains a broad range of nanoparticles with a pulsed laser results in the fragmentation of the nanoparticles, as well as the potential formation of alloyed NPs. Alloy NPs are formed when two individual NPs are brought into close proximity to one another while they are still in a molten state [48].

3. Results and Discussion

3.1. LIBS Spectrum of Bulk Alloy Fabricated Via the Arc Melting Technique

The LIBS technique makes use of the atomic emission spectroscopy of laser generated plasma in order to determine the elemental composition contents of the target. A target material is targeted by a high power laser, and a fraction of the target material is evaporated and ionized to produce plasma with a high pressure and temperature. Radiation that is distinctive of the elements present is emitted when the plasma starts to cool, and this radiation is recorded to generate a spectrum. This is subsequently used to find out about the sample's composition [49,50]. As a potential analytical technique for both quantitative and qualitative analysis, LIBS has drawn more and more interest over the past several decades. The following are some major benefits of LIBS above the traditional methods, particularly when used to study multielement examination [51], there is no need for sample preparation [52], remote analysis is performed in situ [53], data are acquired in real-time [54], and there are only extremely small degrees of damage to the target materials [55]. The composition of bulk alloy synthesized using the arc-melting technique was studied using the LIBS method. Copper and cobalt elements were found from the laser induced plasma of the bulk alloy and LIBS spectrum is presented in Figure 3. The plasma parameters were also determined.
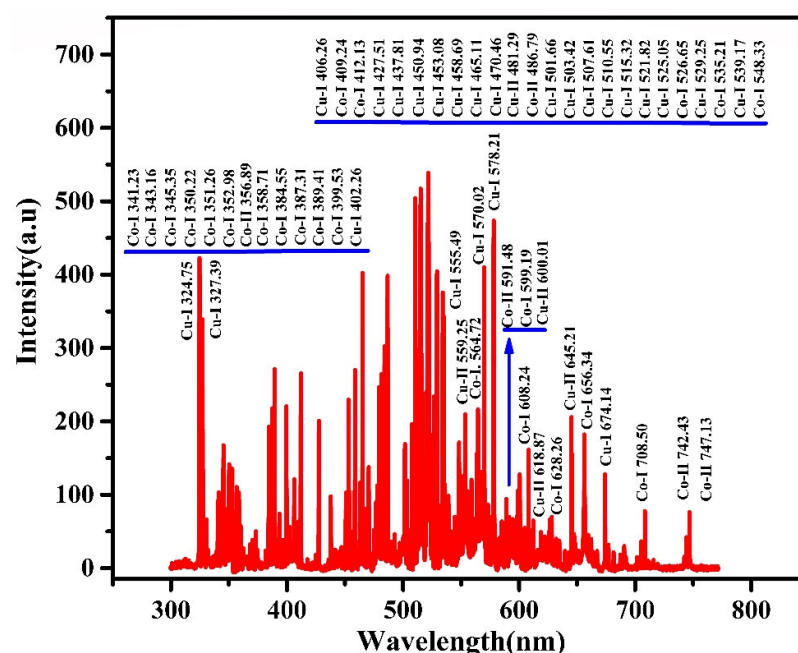

Figure 3. LIBS spectrum of arc-melting assisted synthesis of bulk alloy.

3.2. X-ray Diffraction Pattern of $CuCo_2O_4$ NPs

The X-ray diffraction pattern of $CuCo_2O_4$ nanoparticles synthesized via laser ablation is shown in Figure 4. Following the collection of X-ray powder diffraction data, it was found that copper-cobalt bimetallic particles showed diffraction peaks at 38.4, 44.5, and 65.1°, respectively, which correspond to the (222), (400), and (440) planes. $CuCo_2O_4$ nanoparticles displayed diffraction peaks at 38.3, 44.5, and 65.0° in the (222), (400), and (440) diffraction planes (PDF#76-1887) [56]. XRD characteristic diffraction peaks with minor differences, such as 38.3, 44.6, and 65.1°, corresponding to (222), (400), and (440) for $CuCo_2O_4$ particles

have been reported in [57]. Diffraction peaks for $CuCo_2O_4$ nanoparticles have been found at 38.6, 44.8, and 65.2°, and they belong to (222), (400), and (440) planes, respectively [58–60].
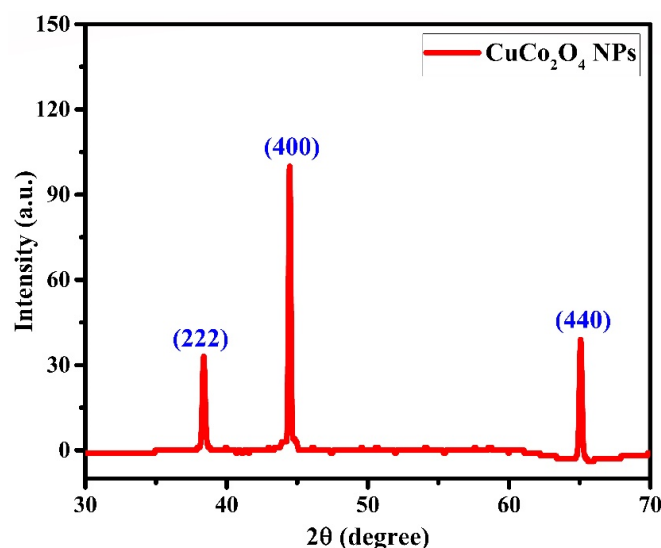

Figure 4. X-ray diffraction pattern of $CuCo_2O_4$ nanoparticles.

3.3. VSM Study of Laser Assisted $CuCo_2O_4$ NPs

Figure 5 demonstrates the results of a study of magnetic hysteresis, that was performed for $CuCo_2O_4$ particles using the VSM technique. It was found that the nanomaterials synthesized via the laser ablation technique had a saturation magnetization of 1.64 emu/g, a coercivity of 424 Oe, and a magnetic remanence of 0.016 emu/g. Researchers found that copper doping is a useful tool for controlling the magnetic characteristics of a parent material by studying how the values of remanent magnetization, coercivity and saturation magnetization change as a function of the ratio of copper content. Thus, grain size, ion distribution, lattice distortion, and condensation may all have a role in the observed difference in magnetic properties [61]. It was found that there was a lower saturation magnetization than expected, and this was due to the fact that there was less amount of material present [62]. Furthermore, the NPs' coercivity is influenced by several factors, including internal forces, particle size, secondary phases, magnetocrystalline anisotropy, lattice defects, and dislocations [63]. Saturation magnetization and coercivity are related to heat generation by the magnetic nanoparticles under alternating magnetic field.

3.4. SEM and EDX Results of $CuCo_2O_4$ NPs Synthesized Via Laser Ablation

The morphology of nanoparticles was examined using SEM. Figure 6a depicts the spherical structure of particles with a diameter of 219 nm that have tiny particles attached to them. The laser-assisted synthesized particles' composition was determined by EDX analysis, and the corresponding spectrum is shown in Figure 6b. The copper, cobalt, and oxygen peaks were seen, and it is possible that the carbon-coated SEM grid would be responsible for the detection of a small peak of carbon. The EDX spectrum showed that there were significant peaks of cobalt, copper, and oxygen. The results of the EDX are presented in Table 1, which may be seen below. Cl originated from the used precursor, while Si, In, Na, Ca, and Mg originating from the indium tin oxide substrate have been observed [64].

3.5. TEM Image and Corresponding Histogram of $CuCo_2O_4$ NPs

Moreover, transmission electron microscopy was used to examine the size and shape of synthesized $CuCo_2O_4$ nanoparticles, as shown in Figure 7a, and the corresponding histogram is presented in Figure 7b. The average particle size is 32 nm, as seen by the histogram of the TEM image. The reported size of particles is 30–90 nm [60], while the

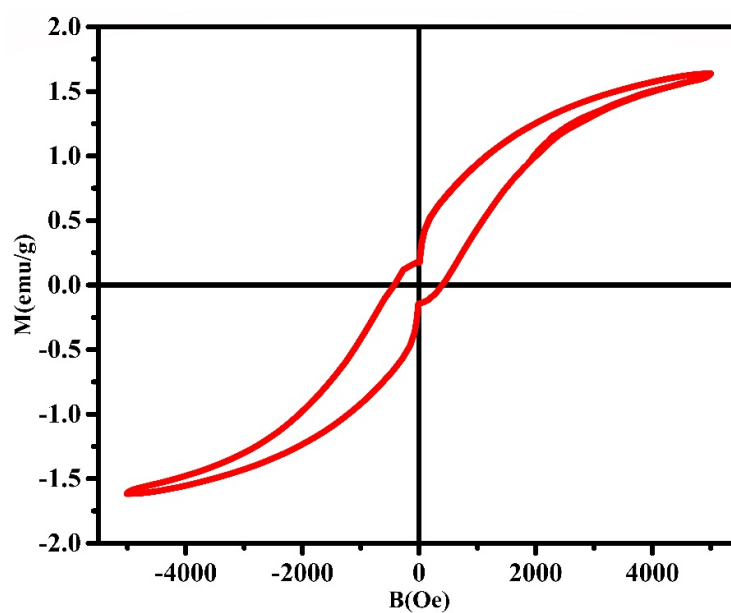average diameter of spherical microstructures is 20 nm [58], and the size of nanorods is 10–20 nm [65].

Figure 5. Magnetic hysteresis loop of $CuCo_2O_4$ nanoparticles.

Figure 6. (**a**) shows the SEM of laser synthesized NPs and (**b**) represents the EDX spectrum.

Table 1. EDX analysis of the laser assisted synthesis of $CuCo_2O_4$.

Element	Line Type	Apparent Concentration	k Ratio	Wt%	Wt% Sigma	Standard Label	Factory Standard
C	K series	0.59	0.00592	4.35	1.03	C Vit	Yes
O	K series	21.43	0.07211	20.7	0.62	SiO2	Yes
Co	K series	9.02	0.09016	15.16	0.81	Co	Yes
Cu	L series	20.96	0.20956	59.79	1.06	Cu	Yes
Total:				100			

Figure 7. (**a**) shows the TEM of laser synthesized NPs and (**b**) represents the corresponding histogram.
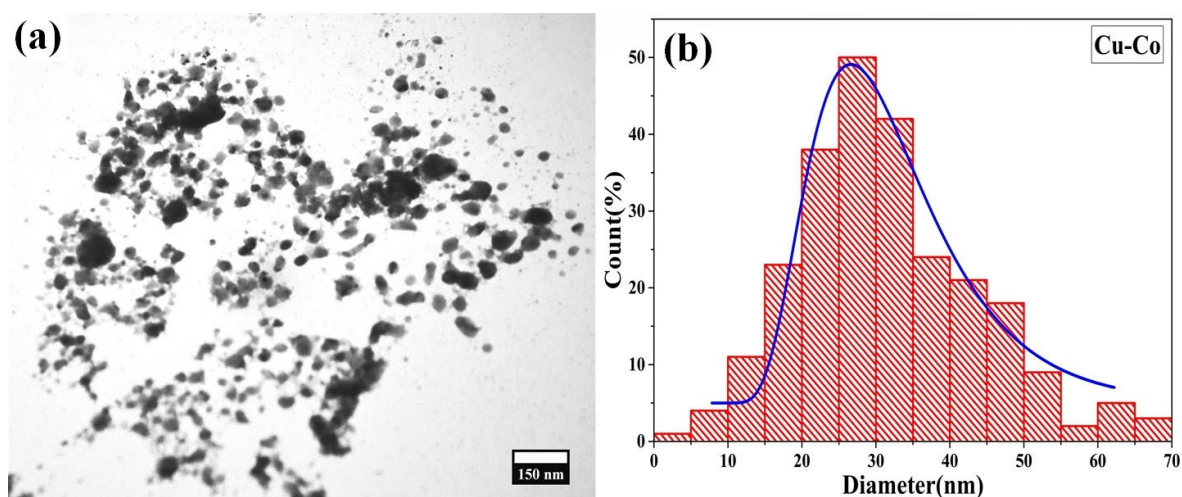
3.6. Dynamic Light Scattering Analysis of $CuCo_2O_4$ NPs

The hydrodynamic size of the nanofluid was recorded using dynamic light scattering, as shown in Figure 8. The hydrodynamic size of the nanoparticles produced via the laser ablation technique was found to be 28 nm. The polydispersity value for this sample was estimated to be 0.222. The polydispersity index determines the extent to which nanoparticles are of similar size [66].
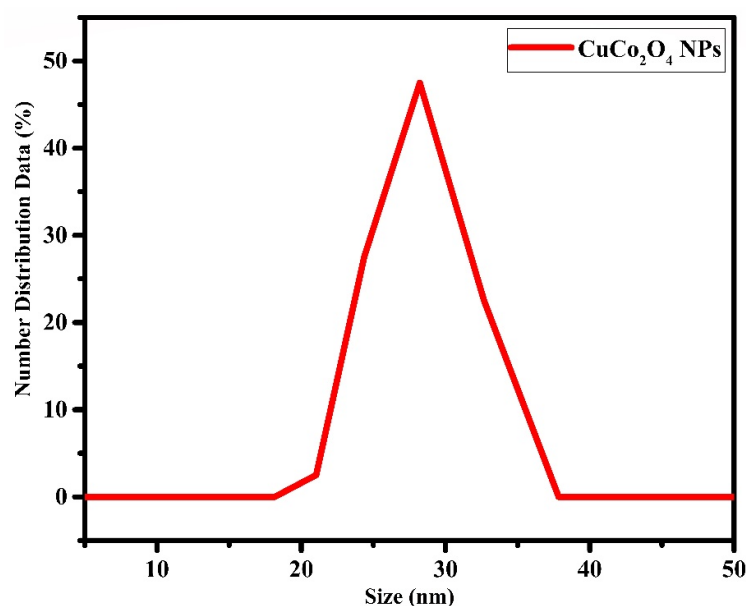

Figure 8. DLS analysis of the laser fabricated $CuCo_2O_4$ nanoparticles.

3.7. Antibacterial Activities of $CuCo_2O_4$ NPs

The precise mechanisms of the nanostructure's toxicity against different bacterial strains are not well known. NPs have the capacity to cling to bacteria. Low pH, high aeration, and high temperature all work against agglomeration to promote toxicity. For antibacterial applications, separate copper and cobalt nanostructures have been studied. As the quantity of agglomeration is lower, there is more surface area available to interact with bacterial cell membrane and solubilize copper ions, this results in increased toxicity. Copper in both its metallic and ionic forms generates hydroxyl radicals, which damage essential DNA and proteins [67]. The significant toxicity of CuO against *E. coli*, *S. aureus*, and *B. subtilis* strains has been demonstrated [68]. Improved bactericidal activity was seen

in hydroxyapatite that had been doped with cobalt. It has not yet been determined how exactly cobalt kills bacteria; however, it is known that cobalt particularly affects DNA polymerization, that further damages DNA [69]. When cobalt binds to DNA, it may change the topology of the DNA and prevent DNA-binding proteins from functioning properly. This can have a negative impact on the efficiency of the DNA replication, repair, and transcription process. Additionally, cobalt is well-known to produce reactive oxygen constituents, which are responsible for the death of bacteria [70]. Cobalt nanomaterials have been proven to have antibacterial activity against different bacterial strains [71–73]. The phenomenon of targeting bactericidal nanostructures to particular bacteria or particular diseased tissue reduces side effects and boosts antibacterial activity, making it a promising approach for the treatment of infection [74]. Multifunctional nanomaterials may be quite helpful in this situation; for example, $Fe_3O_4@TiO_2$ magnetic particles can effectively target various pathogenic bacteria and have effective antibacterial effect [75]. Magnetic hyperthermia and antibacterial properties of $CuCo_2O_4$ nanoparticles synthesized by laser ablation were studied in this research.

Figure 9 shows the results of a study employing the conventional agar well diffusion method to examine the antibacterial properties of $CuCo_2O_4$ nanoparticles [76] against strains of *S. aureus* (Gram-negative and -positive) and *E.coli* (Gram-negative and -positive). Both the positive and negative control groups showed an inhibition zone of 10 ± 0.4 mm when tested against *S.aureus* strains. However, when tested against *E. coli* strains, the inhibition zones recorded 13 ± 0.3 and 12 ± 0.3 mm for the positive and negative controls, respectively. The disruption of cell metabolism or the leaking of plasma after the insertion of the nanoparticles into the bacterial cell may both be used to explain the antibacterial activity of the produced nanoparticles [77,78]. When nanoparticles attacked cell organelles and caused cell line dissociations in bacteria, their normal metabolic activity might be disturbed. This led to cytoplasm leakage, which led to bacterial cell death and irregular expansion of the inhibitory process [79]. The schematic diagram in Figure 10, which was obtained from [80], illustrates how the bimetallic NPs exhibit their antibacterial action.
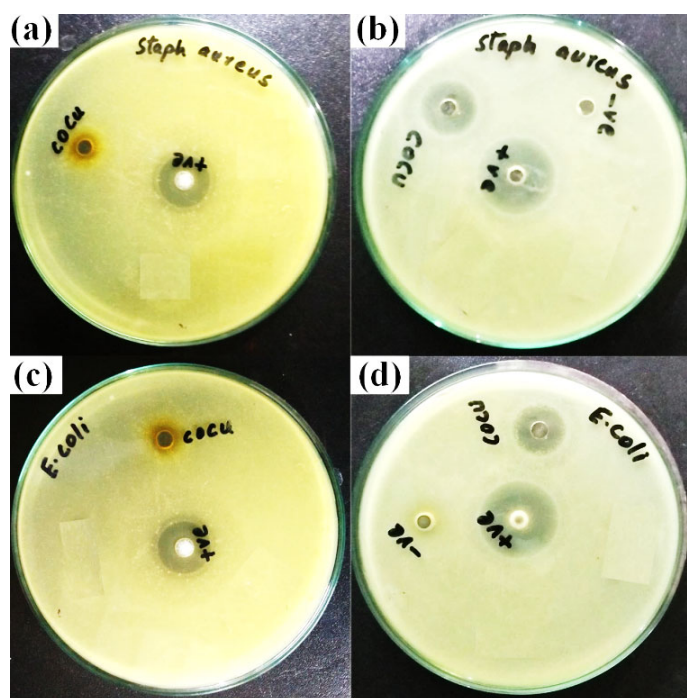

Figure 9. (**a**,**b**) display of the inhibition zone (mm) of $CuCo_2O_4$ NPs against *S.aureus* for positive and negative controls and images (**c**,**d**) against *E.coli* for the positive and negative controls.
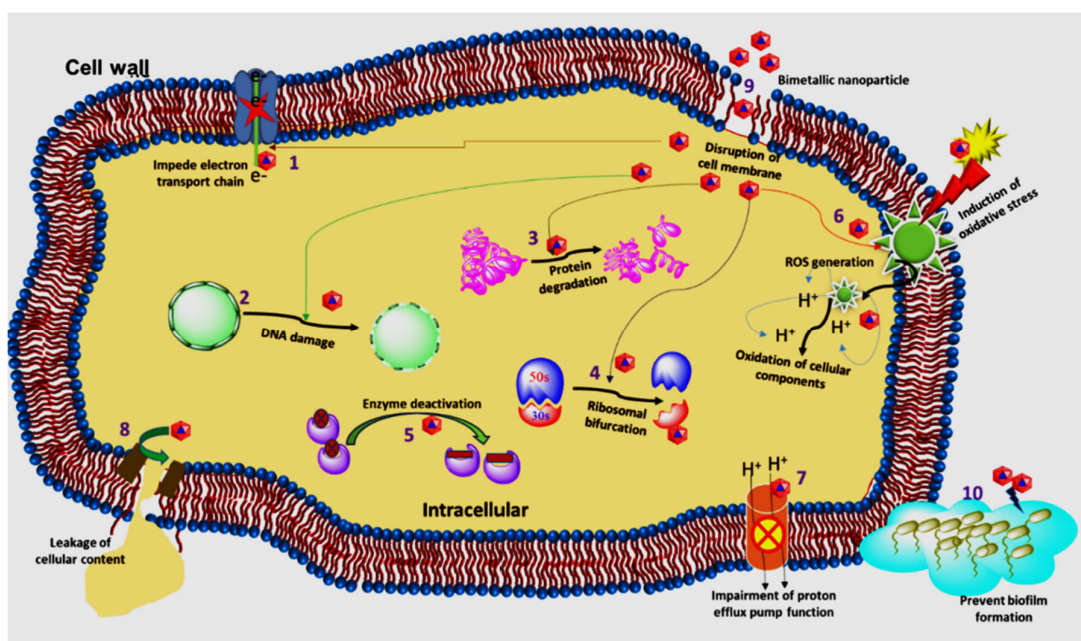
Figure 10. Schematic diagram, which was obtained from [80], illustrates how the bimetallic NPs exhibit their antibacterial action.

3.8. Mutagenicity by Ames Assay of CuCo2O4 Nanoparticles

The mutagenicity of synthesized nanomaterials was evaluated using the Ames test in accordance with the method described in the relevant reference [81]. *Salmonella Typhimurium: TA-100* and *TA-98* mutant strains were used to assess the mutagenicity of NPs. The test, background, and control plates were recorded visually. Purple wells were classed as negative wells, whereas partially and entirely yellow wells were considered positive wells. If the test plate wells turned purple, it meant the material is harmful to the test strain [82,83]. A fluctuation approach performed entirely in liquid culture was used to examine the gene mutation frequency and carcinogenicity. The color shifts of the sample wells were compared to those of the background wells. It was observed that $CuCo_2O_4$ particles synthesized through laser ablation method showed non-mutagenic capability against both *S.typhimurium TA-98* and *TA-100*. Table 2 summarizes the results of the mutagenic activity. If the number of positive wells in the sample doubles when compared to the background, the sample is deemed to be mutagenic [81].

Table 2. Mutagenic activity of $CuCo_2O_4$ nanoparticles.

Samples	Number of Positive Wells/Number of Total Wells			
	S. typhimurium TA-98	Results	*S. typhimurium TA-100*	Results
Blank	0/96	Non-mutagenic	0/96	Non-mutagenic
Standard	78/96	Mutagenic	84/96	Mutagenic
Background	20/96	-	23/96	-
$CuCo_2O_4$ NPs	30/96	Non-mutagenic	38/96	Non-mutagenic

3.9. Magnetic Fluid Hyperthermia Study of Laser Synthesized CuCo2O4 Nanofluid

A lab-made magnetic setup was used to study the magnetic fluid hyperthermia of the synthesized $CuCo_2O_4$ nanofluid, and the schematic diagram is shown in Figure 11, as previously described in our work [26]. The rate of increase in temperature over time for the nanoparticles was studied in order to probe into the self-heating properties of particles for the magnetic hyperthermia, as shown in Figure 12.
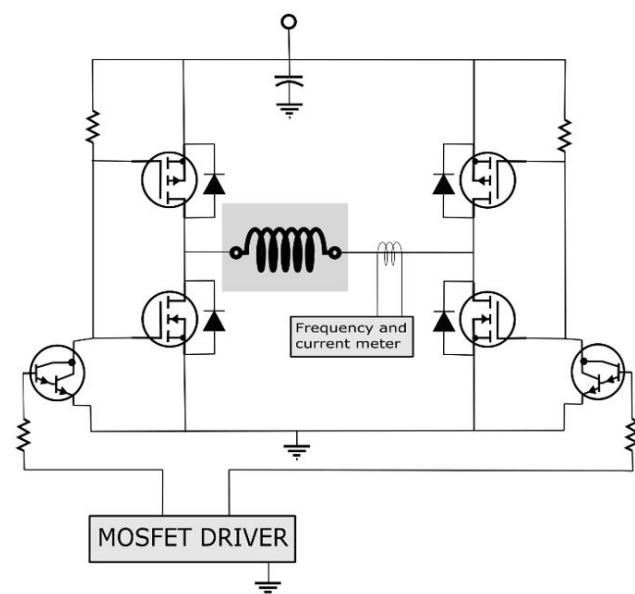
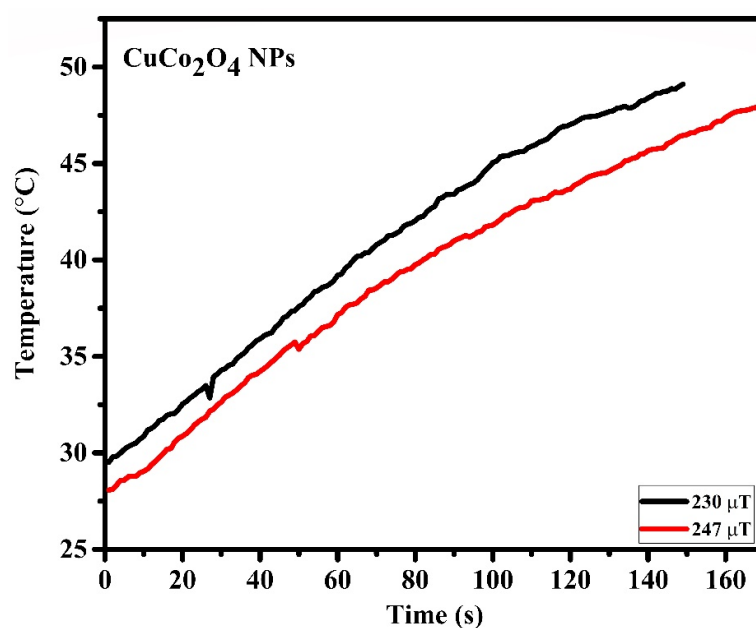**Figure 11.** Shows the schematic diagram of magnetic hyperthermia.

Figure 12. Induction heating profile of time vs. temperature of $CuCo_2O_4$ nanoparticles.

The specific absorption rate (SAR) was recorded using the Equation (1) and SAR, defined as the amount of heat generated by the material per unit mass per unit of time, has been studied to gain insight into the heating capability of the magnetic sample [84,85]. The magnetic field intensity and frequency, the concentration of NPs, their shape, size, polydispersity, type, and the ferro-fluid chemical and physical properties are all known to affect the SAR [86]. According to a comprehensive study of magnetic hyperthermia conducted by various studies, the acceptable frequency range ranges from 10 kHz to 1 GHz [87,88], while the magnetic field's amplitude may vary from 10 Oe to 1000 Oe [89,90].

$$SAR = C_p \frac{\Delta T}{\Delta t} \frac{m_s}{m_n} \tag{1}$$

In Equation (1), m_n mass of the nanoparticles, m_s mass of the solution, C_p, is the specific heat of solution, 4184 J·kg^{-1}·K^{-1}, and $\frac{\Delta T}{\Delta t}$ is the initial slope of the heating curve.

During magnetic fields of 230 and 247 µT, respectively, the specific absorption rates of 4.57 and 5.17 W/g were measured. The temperature of the sample initially begins to rise during the course of the experiment, but it eventually reaches a point where it is stable. This is because the heat that is generated by the nanoparticles is absorbed by the medium that is being used [91]. Recently, our group has reported the copper-iron and copper-nickel NPs for magnetic hyperthermia study synthesized using the laser ablation technique. For the copper-nickel nanomaterials, the SAR values of 5.04 and 2.18 W/g were reported, whereas the SAR values for the copper-iron nanomaterials were 9.74 and 7.39 W/g measured [26].

Magnetic Heating Mechanism

In general, Brownian relaxation and Néel relaxation, hysteresis loss and eddy currents are the four independent processes that can cause heating in magnetic nanoparticles, when exposed to high frequency magnetic fields. Eddy currents are not relevant for nanomaterial hyperthermia [92]. If a nanoparticle rotates as a consequence of this rotation, the nanoparticle has experienced Brownian relaxation and heat energy is transferred via shear stress in the fluid around it. Magnetic moment rotation without particle motion indicates Néel relaxation, and heat energy is released by the reorganization of atomic dipole moments in a crystal. In actual situations, both of these mechanisms could take place at the same time. However, an externally supplied magnetic field could give sufficient energy to shift the moments from its preferred direction. When the moment returns to equilibrium, this leads to the discharge of thermal energy, which causes local heating [18]. There have been many factors that may affect the magnetic nanoparticles' heating efficiencies. As predicted, investigations reveal that the specific absorption rate (SAR) rises with the rising field strength, and the loss of power in the magnetic hyperthermia is proportional to the square of amplitude of the magnetic field [93–95]. The magnetic nanoparticles may generate thermal energy by following hysteresis loss, Brownian relaxation, and Néel relaxation, and exactly which of these mechanisms dominates depends largely on the size of the particle. In big particles, hysteresis losses predominate [93]. Anisotropy energy is the amount of energy needed to move a nanoparticle's magnetic moment away from its preferred axis. Brownian rotation is made possible by this energy barrier. However, in Néel relaxation, where it has a huge impact on SAR due to its exponential effect on relaxation time, anisotropy plays a more prominent role. Controlling magnet anisotropy of the component particles in a particle system is thus very necessary in order to successfully optimize such a system for use in hyperthermia therapeutics. The higher nanoparticle concentrations needed for efficient hyperthermia can lead to systems with strong interactions. Therefore, measuring heating efficiency requires a thorough knowledge of the collective behavior of the particle systems in their entirety. Based on certain research, collective behavior may have a significant impact on SAR [18,93,96].

4. Conclusions

The bimetallic copper-cobalt alloy was fabricated using arc-melting technique and was analyzed using laser induced breakdown spectroscopy. This alloy was subsequently used to synthesize $CuCo_2O_4$ NPs using the environmentally friendly and contamination-free laser ablation technique. The TEM image showed that NPs were of spherical shape with an average size of 32 nm, while the DLS analysis showed hydrodynamic diameters of 28 nm. The synthesized NPs exhibited antibacterial activities. Both the positive and negative control groups showed an inhibition zone of 10 ± 0.4 mm when tested against *S.aureus* strains. For the positive and negative controls against the *E. coli* strain, the zones of inhibition were recorded as 13 ± 0.3 and 12 ± 0.3 mm, respectively. Further, nanomaterials showed non-mutagenic capability against both *S. typhimurium TA-98* and *TA-100* mutant strains. Finally, with magnetic fields of 230 and 247 µT, respectively, the specific absorption rates of 4.57 and 5.17 W/g were recorded. The results of the study on magnetic hyperthermia and antibacterial activity show that the synthesized nanoparticles can potentially be used in the treatment of cancer, as well as several other biological fields.

Institutional Review Board Statement: Not Applicable.

Informed Consent Statement: Not Applicable.

Data Availability Statement: The data that support the findings of this study are available from the corresponding author upon reasonable request.

Conflicts of Interest: The authors declare no conflict of interest.

References

1. Sheikhi Mehrabadi, Z.; Ahmadpour, A.; Shahtahmasebi, N.; Bagheri Mohagheghi, M.M. Synthesis and Characterization of Cu Doped Cobalt Oxide Nanocrystals as Methane Gas Sensors. *Phys. Scr.* **2011**, *84*, 015801. [CrossRef]
2. Shah, A.A.; Bhatti, M.A.; Tahira, A.; Chandio, A.D.; Channa, I.A.; Sahito, A.G.; Chalangar, E.; Willander, M.; Nur, O.; Ibupoto, Z.H. Facile synthesis of copper doped ZnO nanorods for the efficient photo degradation of methylene blue and methyl orange. *Ceram. Int.* **2020**, *46*, 9997–10005. [CrossRef]
3. Maliha, Z.; Rani, M.; Neffati, R.; Mahmood, A.; Iqbal, M.Z.; Shah, A. Investigation of copper/cobalt MOFs nanocomposite as an electrode material in supercapacitors. *Int. J. Energy Res.* **2022**, *46*, 17404–17415. [CrossRef]
4. Anithkumar, M.; Rajan, S.A.; Khan, A.; Kaczmarek, B.; Michalska-Sionkowska, M.; Łukowicz, K.; Osyczka, A.M.; Gupta, J.; Sahu, N.K. Glucose Oxidase-Loaded $MnFe_2O_4$ Nanoparticles for Hyperthermia and Cancer Starvation Therapy. *ACS Appl. Nano Mater.* **2023**, *6*, 2605–2614. [CrossRef]
5. Ahmed, K.; Zaidi, S.F. Treating Cancer with Heat: Hyperthermia as Promising Strategy to Enhance Apoptosis. *J. Pak. Med. Assoc.* **2013**, *63*, 504–508.
6. Brezovich, I.A.; Young, J.H. Hyperthermia with Implanted Electrodes. *Med. Phys.* **1981**, *8*, 79–84. [CrossRef]
7. Robins, H.I.; Rushing, D.; Kutz, M.; Tutsch, K.D.; Tiggelaar, C.L.; Paul, D.; Spriggs, D.; Kraemer, C.; Gillis, W.; Feierabend, C.; et al. Phase I Clinical Trial of Melphalan and 41.8 °C Whole-Body Hyperthermia in Cancer Patients. *J. Clin. Oncol.* **1997**, *15*, 158–164. [CrossRef]
8. Douple, E.B.; Strohbehn, J.W.; Bowers, E.D.; Walsh, J.E. Cancer Therapy with Localized Hyperthermia Using an Invasive Microwave System. *J. Microw. Power* **1979**, *14*, 181–186. [CrossRef]
9. Tishin, A.; Shtil, A.; Pyatakov, A.; Zverev, V. Developing Antitumor Magnetic Hyperthermia: Principles, Materials and Devices. *Recent Pat. Anticancer Drug Discov.* **2016**, *11*, 360–375. [CrossRef]
10. Dutz, S.; Hergt, R. Magnetic Particle Hyperthermia—A Promising Tumour Therapy? *Nanotechnology* **2014**, *25*, 452001. [CrossRef]
11. Gilchrist, R.K.; Medal, R.; Shorey, W.D.; Hanselman, R.C.; Parrott, J.C.; Taylor, C.B. Selective Inductive Heating of Lymph Nodes. *Ann. Surg.* **1957**, *146*, 596–606. [CrossRef]
12. Kumar, C.S.S.R.; Mohammad, F. Magnetic Nanomaterials for Hyperthermia-Based Therapy and Controlled Drug Delivery. *Adv. Drug Deliv. Rev.* **2011**, *63*, 789–808. [CrossRef]
13. Nasrin, S.; Chowdhury, F.U.Z.; Hoque, S.M. Study of Hydrodynamic Size Distribution and Hyperthermia Temperature of Chitosan Encapsulated Zinc-Substituted Manganese Nano Ferrites Suspension. *Phys. B Condens. Matter* **2019**, *561*, 54–63. [CrossRef]
14. Ghayour, H.; Abdellahi, M.; Ozada, N.; Jabbrzare, S.; Khandan, A. Hyperthermia Application of Zinc Doped Nickel Ferrite Nanoparticles. *J. Phys. Chem. Solids* **2017**, *111*, 464–472. [CrossRef]
15. Suleman, M.; Riaz, S. In Silico Study of Hyperthermia Treatment of Liver Cancer Using Core-Shell $CoFe_2O_4$@$MnFe_2O_4$ Magnetic Nanoparticles. *J. Magn. Magn. Mater.* **2020**, *498*, 166143. [CrossRef]
16. Shah, S.A.; Hashmi, M.U.; Alam, S.; Shamim, A. Magnetic and Bioactivity Evaluation of Ferrimagnetic $ZnFe_2O_4$ Containing Glass Ceramics for the Hyperthermia Treatment of Cancer. *J. Magn. Magn. Mater.* **2010**, *322*, 375–381. [CrossRef]
17. Ban, I.; Stergar, J.; Drofenik, M.; Ferk, G.; Makovec, D. Synthesis of Copper-Nickel Nanoparticles Prepared by Mechanical Milling for Use in Magnetic Hyperthermia. *J. Magn. Magn. Mater.* **2011**, *323*, 2254–2258. [CrossRef]
18. Deatsch, A.E.; Evans, B.A. Heating Efficiency in Magnetic Nanoparticle Hyperthermia. *J. Magn. Magn. Mater.* **2014**, *354*, 163–172. [CrossRef]
19. Akurati, R.R.; Jaladi, N.K.; Kurapati, S.R.; Kapusetti, G.; Choppadandi, M.; Mandal, P. Preparation, Characterization and Study of Magnetic Induction Heating of Co-Cu Nanoparticles. *Mater. Today Commun.* **2023**, *34*, 104964. [CrossRef]

20. Jamir, M.; Borgohain, C.; Borah, J.P. Study of Chitosan Coated Copper Substituted Nano-Ferrites for Hyperthermia Applications. *Phys. E Low-Dimens. Syst. Nanostruct.* **2023**, *146*, 115560. [CrossRef]
21. Kim, D.H.; Nikles, D.E.; Johnson, D.T.; Brazel, C.S. Heat Generation of Aqueously Dispersed CoFe2O4 Nanoparticles as Heating Agents for Magnetically Activated Drug Delivery and Hyperthermia. *J. Magn. Magn. Mater.* **2008**, *320*, 2390–2396. [CrossRef]
22. Fotukian, S.M.; Barati, A.; Soleymani, M.; Alizadeh, A.M. Solvothermal Synthesis of $CuFe_2O_4$ and Fe_3O_4 Nanoparticles with High Heating Efficiency for Magnetic Hyperthermia Application. *J. Alloys Compd.* **2020**, *816*, 152548. [CrossRef]
23. Ben-Nissan, B.; Ka, S.; Himanshu, T.; Huguenin, K.; Sp, S. Structural, magnetic and in vitro bioactivity of co-cu ferrite and bioglass composite for hyperthermia in bone tissue engineering. *Bioceram. Dev. Appl.* **2016**, *2016*, 03794111.
24. Goudarzi, M.; Salavati-Niasari, M.; Yazdian, F.; Amiri, M. Sonochemical Assisted Thermal Decomposition Method for Green Synthesis of $CuCo_2O_4$/CuO Ceramic Nanocomposite Using Dactylopius Coccus for Anti-Tumor Investigations. *J. Alloys Compd.* **2019**, *788*, 944–953. [CrossRef]
25. Rivera-Chaverra, M.J.; Restrepo-Parra, E.; Acosta-Medina, C.D.; Mello, A.; Ospina, R. Synthesis of Oxide Iron Nanoparticles Using Laser Ablation for Possible Hyperthermia Applications. *Nanomaterials* **2020**, *10*, 2099. [CrossRef] [PubMed]
26. Ali, I.; Pan, Y.; Jamil, Y.; Shah, A.A.; Amir, M.; Al Islam, S.; Fazal, Y.; Chen, J.; Shen, Z. Comparison of Copper-Based Cu-Ni and Cu-Fe Nanoparticles Synthesized via Laser Ablation for Magnetic Hyperthermia and Antibacterial Applications. *Phys. B Condens. Matter* **2023**, *650*, 414503. [CrossRef]
27. Kim, Y.H.; Choi, Y.R.; Kim, K.M.; Choi, S.Y. Evaluation of Copper Ion of Antibacterial Effect on Pseudomonas Aeruginosa, Salmonella Typhimurium and Helicobacter Pylori and Optical, Mechanical Properties. *Appl. Surf. Sci.* **2012**, *258*, 3823–3828. [CrossRef]
28. Ramesh, J.; Carter, A.O.; Campbell, M.H.; Gibbons, N.; Powlett, C.; Moseley, H.; Lewis, D.; Carter, T. Use of Mobile Phones by Medical Staff at Queen Elizabeth Hospital, Barbados: Evidence for Both Benefit and Harm. *J. Hosp. Infect.* **2008**, *70*, 160–165. [CrossRef]
29. Brady, R.R.W.; Verran, J.; Damani, N.N.; Gibb, A.P. Review of Mobile Communication Devices as Potential Reservoirs of Nosocomial Pathogens. *J. Hosp. Infect.* **2009**, *71*, 295–300. [CrossRef]
30. Esteban-Tejeda, L.; Malpartida, F.; Esteban-Cubillo, A.; Pecharromán, C.; Moya, J.S. The Antibacterial and Antifungal Activity of a Soda-Lime Glass Containing Silver Nanoparticles. *Nanotechnology* **2009**, *20*, 085102. [CrossRef]
31. Dabagh, S.; Chaudhary, K.; Haris, S.A.; Haider, Z.; Ali, J. Aluminium Substituted Ferrite Nanoparticles with Enhanced Antibacterial Activity. *J. Comput. Theor. Nanosci.* **2018**, *15*, 1052–1058. [CrossRef]
32. Kumar, P.; Mathpal, M.C.; Ghosh, S.; Inwati, G.K.; Maze, J.R.; Duvenhage, M.M.; Roos, W.D.; Swart, H.C. Plasmonic Au Nanoparticles Embedded in Glass: Study of TOF-SIMS, XPS and Its Enhanced Antimicrobial Activities. *J. Alloys Compd.* **2022**, *909*, 164789. [CrossRef]
33. Paknahad, P.; Askari, M.; Ghorbanzadeh, M. Application of Sol-Gel Technique to Synthesis of Copper-Cobalt Spinel on the Ferritic Stainless Steel Used for Solid Oxide Fuel Cell Interconnects. *J. Power Sources* **2014**, *266*, 79–87. [CrossRef]
34. Bhatti, A.M.; Almaani, K.F.; Shah, A.A.; Tahira, A.; Chandio, A.D.; Mugheri, A.Q.; Bhatti, A.L. Low Temperature Aqueous Chemical Growth Method for the Doping of W into ZnO Nanostructures and Their Photocatalytic Role in the Degradration of Methylene Blue. *J. Clust. Sci.* **2022**, *33*, 1445–1446. [CrossRef]
35. Bhatti, M.A.; Gilani, S.J.; Shah, A.A.; Channa, I.A.; Almani, K.F.; Chandio, A.D.; Halepoto, I.A.; Tahira, A.; Bin Jumah, M.N.; Ibupoto, Z.H. Effective removal of methylene blue by surface alteration of TiO2 with Ficus Carica leaf extract under visible light. *Nanomaterials* **2022**, *12*, 2766. [CrossRef]
36. Akhtar, N.; Rani, M.; Mahmood, A.; Tariq, K.; Murtaza, G.; Alothman, A.A.; AL-zahrani, R.S.; Ali, S.; Janjua, N.K.; Shah, A. Synthesis and characterization of graphene oxide-based nanocomposite $NaCr_2O_4$/GO for electrochemical applications. *J. Mater. Res. Technol.* **2021**, *15*, 6287–6294. [CrossRef]
37. Xiao, X.; Zhang, Z.; Cai, L.; Li, Y.; Yan, Z.; Wang, Y. The Excellent Catalytic Activity for Thermal Decomposition of Ammonium Perchlorate Using Porous $CuCo_2O_4$ Synthesized by Template-Free Solution Combustion Method. *J. Alloys Compd.* **2019**, *797*, 548–557. [CrossRef]
38. Manikandan, A.; Sridhar, R.; Arul Antony, S.; Ramakrishna, S. A Simple Aloe Vera Plant-Extracted Microwave and Conventional Combustion Synthesis: Morphological, Optical, Magnetic and Catalytic Properties of CoFe2O4 nanostructures. *J. Mol. Struct.* **2014**, *1076*, 188–200. [CrossRef]
39. Chen, L.; Hong, M. Functional Nonlinear Optical Nanoparticles Synthesized by Laser Ablation. *Opto-Electron. Sci.* **2022**, *1*, 210007. [CrossRef]
40. Amendola, V.; Meneghetti, M. What Controls the Composition and the Structure of Nanomaterials Generated by Laser Ablation in Liquid Solution? *Phys. Chem. Chem. Phys.* **2013**, *15*, 3027–3046. [CrossRef]
41. Zhang, D.; Gökce, B.; Barcikowski, S. Laser Synthesis and Processing of Colloids: Fundamentals and Applications. *Chem. Rev.* **2017**, *117*, 3990–4103. [CrossRef] [PubMed]
42. Zhang, D.S.; Liu, J.; Liang, C.H. Perspective on How Laser-Ablated Particles Grow in Liquids. *Sci. China Physics Mech. Astron.* **2017**, *60*, 074201. [CrossRef]
43. Liu, J.; Gong, Y.; Xu, G.; Peng, G.; Shah, I.A.; Ul Hassan, N.; Xu, F. Realization of Magnetostructural Coupling by Modifying Structural Transitions in MnNiSi-CoNiGe System with a Wide Curie-Temperature Window. *Sci. Rep.* **2016**, *6*, 23386. [CrossRef] [PubMed]

44. Khan, M.; Nowsherwan, G.A.; Shah, A.A.; Riaz, S.; Riaz, M.; Chandio, A.D.; Shah, A.K.; Channa, I.A.; Hussain, S.S.; Ali, R.; et al. A Study of the Structural and Surface Morphology and Photoluminescence of Ni-Doped AlN Thin Films Grown by Co-Sputtering. *Nanomaterials* **2022**, *12*, 3919. [CrossRef] [PubMed]

45. Shukri, W.N.W.; Bidin, N.; Islam, S.; Krishnan, G. Synthesis of Au–Ag Alloy Nanoparticles in Deionized Water by Pulsed Laser Ablation Technique. *J. Nanosci. Nanotechnol.* **2018**, *18*, 4841–4851. [CrossRef]

46. Santagata, A.; National, I.; Guarnaccio, A.; National, I.; Valyon, J. Production of Silver-Silica Core-Shell Nanocomposites Using Ultra-Short Pulsed Laser Ablation in Nanoporous Aqueous Silica Colloidal Solutions. *J. Phys. D Appl. Phys.* **2015**, *48*, 205304. [CrossRef]

47. Ibupoto, Z.H.; Tahira, A.; Shah, A.A.; Aftab, U.; Solangi, M.Y.; Leghari, J.A.; Samoon, A.H.; Bhatti, A.L.; Bhatti, M.A.; Mazzaro, R.; et al. NiCo$_2$O$_4$ nanostructures loaded onto pencil graphite rod: An advanced composite material for oxygen evolution reaction. *Int. J. Hydrog. Energy* **2022**, *47*, 6650–6665. [CrossRef]

48. Serkov, A.A.; Kuzmin, P.G.; Shafeev, G.A. Laser-Induced Agglomeration of Gold and Silver Nanoparticles Dispersed in Liquid. *Chem. Phys. Lett.* **2016**, *647*, 68–72. [CrossRef]

49. Hahn, D.W.; Omenetto, N. Laser-Induced Breakdown Spectroscopy (LIBS), Part I: Review of Basic Diagnostics and Plasmaparticle Interactions: Still-Challenging Issues within the Analytical Plasma Community. *Appl. Spectrosc.* **2010**, *64*, 335–366. [CrossRef]

50. Limbeck, A.; Brunnbauer, L.; Lohninger, H.; Pořízka, P.; Modlitbová, P.; Kaiser, J.; Janovszky, P.; Kéri, A.; Galbács, G. Methodology and Applications of Elemental Mapping by Laser Induced Breakdown Spectroscopy. *Anal. Chim. Acta* **2021**, *1147*, 72–98. [CrossRef]

51. Takahashi, T.; Thornton, B.; Ohki, K.; Sakka, T. Calibration-Free Analysis of Immersed Brass Alloys Using Long-Ns-Duration Pulse Laser-Induced Breakdown Spectroscopy with and without Correction for Nonstoichiometric Ablation. *Spectrochim. Acta Part B At. Spectrosc.* **2015**, *111*, 8–14. [CrossRef]

52. Jantzi, S.C.; Motto-Ros, V.; Trichard, F.; Markushin, Y.; Melikechi, N.; De Giacomo, A. Sample Treatment and Preparation for Laser-Induced Breakdown Spectroscopy. *Spectrochim. Acta Part B At. Spectrosc.* **2016**, *115*, 52–63. [CrossRef]

53. Bol'shakov, A.A.; Yoo, J.H.; Liu, C.; Plumer, J.R.; Russo, R.E. Laser-Induced Breakdown Spectroscopy in Industrial and Security Applications. *Appl. Opt.* **2010**, *49*, C132–C142. [CrossRef]

54. Hahn, D.W.; Omenetto, N. Laser-Induced Breakdown Spectroscopy (LIBS), Part II: Review of Instrumental and Methodological Approaches to Material Analysis and Applications to Different Fields. *Appl. Spectrosc.* **2012**, *66*, 347–419. [CrossRef]

55. Owens, T.; Mao, S.S.; Canfield, E.K.; Grigoropoulos, C.P.; Mao, X.; Russo, R.E. Ultrafast Thin-Film Laser-Induced Breakdown Spectroscopy of Doped Oxides. *Appl. Opt.* **2010**, *49*, 67–69. [CrossRef]

56. Liao, J.; Feng, Y.; Wu, S.; Ye, H.; Zhang, J.; Zhang, X.; Xie, F.; Li, H. Hexagonal CuCo$_2$O$_4$ Nanoplatelets, a Highly Active Catalyst for the Hydrolysis of Ammonia Borane for Hydrogen Production. *Nanomaterials* **2019**, *9*, 360. [CrossRef]

57. Tian, Z.; Vieker, H.; Kouotou, P.; Beyer, A. In Situ Characterization of Cu–Co Oxides for Catalytic Application. *Faraday Discuss.* **2015**, *177*, 249–262. [CrossRef]

58. Silambarasan, M.; Padmanathan, N.; Ramesh, P.S.; Geetha, D. Spinel CuCo$_2$O$_4$ Nanoparticles: Facile One-Step Synthesis, Optical, and Electrochemical Properties. *Mater. Res. Express* **2016**, *3*, 095021. [CrossRef]

59. Bagtache, R.; Boudjedien, K.; Sebai, I.; Meziani, D.; Trari, M. Facile Preparation of the Spinel CuCo$_2$O$_4$ Application to Hydrogen Photo-Production. *Appl. Phys. A Mater. Sci. Process.* **2021**, *127*, 60. [CrossRef]

60. Rahmatolahzadeh, R.; Mousavi-Kamazani, M.; Shobeiri, S.A. Facile Co-Precipitation-Calcination Synthesis of CuCo$_2$O$_4$ Nanostructures Using Novel Precursors for Degradation of Azo Dyes. *J. Inorg. Organomet. Polym. Mater.* **2017**, *27*, 313–322. [CrossRef]

61. Mohamed, W.S.; Hadia, N.M.A.; Al Bakheet, B.; Alzaid, M.; Abu-Dief, A.M. Impact of Cu^{2+} Cations Substitution on Structural, Morphological, Optical and Magnetic Properties of Co1-XCuxFe$_2$O$_4$ Nanoparticles Synthesized by a Facile Hydrothermal Approach. *Solid State Sci.* **2022**, *125*, 106841. [CrossRef]

62. Tripathi, H.; Pandey, G.C.; Dubey, A.; Shaw, S.K.; Prasad, N.K.; Singh, S.P.; Rath, C. Superparamagnetic Manganese Ferrite and Strontium Bioactive Glass Nanocomposites: Enhanced Biocompatibility and Antimicrobial Properties for Hyperthermia Application. *Adv. Eng. Mater.* **2021**, *23*, 2000275. [CrossRef]

63. Mammo, T.W.; Murali, N.; Sileshi, Y.M.; Arunamani, T. Studies of Structural, Morphological, Electrical, and Magnetic Properties of Mg-Substituted Co-Ferrite Materials Synthesized Using Sol-Gel Autocombustion Method. *Phys. B Condens. Matter* **2017**, *523*, 24–30. [CrossRef]

64. Nwanya, A.C.; Awada, C.; Obi, D.; Raju, K.; Ozoemena, K.I.; Osuji, R.U.; Ruediger, A.; Maaza, M.; Rosei, F.; Ezema, F.I. Nanoporous Copper-Cobalt Mixed Oxide Nanorod Bundles as High Performance Pseudocapacitive Electrodes. *J. Electroanal. Chem.* **2017**, *787*, 24–35. [CrossRef]

65. Samanta, S.; Srivastava, R. Simultaneous Determination of Epinephrene and Paracetamol at Copper-Cobalt Oxide Spinel Decorated Nanocrystalline Zeolite Modified Electrodes. *J. Colloid Interface Sci.* **2016**, *475*, 126–135. [CrossRef]

66. Joshi, A.; Naatz, H.; Faber, K.; Pokhrel, S.; Dringen, R. Iron-Doping of Copper Oxide Nanoparticles Lowers Their Toxic Potential on C6 Glioma Cells. *Neurochem. Res.* **2020**, *45*, 809–824. [CrossRef]

67. Pramanik, A.; Laha, D.; Bhattacharya, D.; Pramanik, P.; Karmakar, P. A Novel Study of Antibacterial Activity of Copper Iodide Nanoparticle Mediated by DNA and Membrane Damage. *Colloids Surf. B Biointerfaces* **2012**, *96*, 50–55. [CrossRef]

68. Baek, Y.W.; An, Y.J. Microbial Toxicity of Metal Oxide Nanoparticles (CuO, NiO, ZnO, and Sb$_2$O$_3$) to *Escherichia Coli*, *Bacillus Subtilis*, and *Streptococcus Aureus*. *Sci. Total Environ.* **2011**, *409*, 1603–1608. [CrossRef]

69. Kumar, V.; Mishra, R.K.; Kaur, G.; Dutta, D. Cobalt and Nickel Impair DNA Metabolism by the Oxidative Stress Independent Pathway. *Metallomics* **2017**, *9*, 1596–1609. [CrossRef]

70. Simonsen, L.O.; Harbak, H.; Bennekou, P. Cobalt Metabolism and Toxicology—A Brief Update. *Sci. Total Environ.* **2012**, *432*, 210–215. [CrossRef]

71. Zaib, M.; Shahzadi, T.; Muzammal, I.; Farooq, U. Catharanthus Roseus Extract Mediated Synthesis of Cobalt Nanoparticles: Evaluation of Antioxidant, Antibacterial, Hemolytic and Catalytic Activities. *Inorg. Nano-Met. Chem.* **2020**, *50*, 1171–1180. [CrossRef]

72. Anuradha, C.T.; Raji, P. Citrus Limon Fruit Juice-Assisted Biomimetic Synthesis, Characterization and Antimicrobial Activity of Cobalt Oxide (Co_3O_4) Nanoparticles. *Appl. Phys. A Mater. Sci. Process.* **2021**, *127*, 949. [CrossRef]

73. Anupong, W.; On-uma, R.; Jutamas, K.; Joshi, D.; Salmen, S.H.; Alahmadi, T.A.; Jhanani, G.K. Cobalt Nanoparticles Synthesizing Potential of Orange Peel Aqueous Extract and Their Antimicrobial and Antioxidant Activity. *Environ. Res.* **2023**, *216*, 114594. [CrossRef]

74. Suri, S.S.; Fenniri, H.; Singh, B. Nanotechnology-Based Drug Delivery Systems. *J. Occup. Med. Toxicol.* **2007**, *2*, 16. [CrossRef]

75. Chen, W.J.; Tsai, P.J.; Chen, Y.C. Functional Fe_3O_4/TiO_2 Core/Shell Magnetic Nanoparticles as Photokilling Agents for Pathogenic Bacteria. *Small* **2008**, *4*, 485–491. [CrossRef]

76. Gonelimali, F.D.; Lin, J.; Miao, W.; Xuan, J.; Charles, F.; Chen, M.; Hatab, S.R. Antimicrobial Properties and Mechanism of Action of Some Plant Extracts against Food Pathogens and Spoilage Microorganisms. *Front. Microbiol.* **2018**, *9*, 1639. [CrossRef]

77. Prakash, J.; Kumar, P.; Harris, R.A.; Swart, C.; Neethling, J.H.; Van Vuuren, A.J.; Swart, H.C. Synthesis, Characterization and Multifunctional Properties of Plasmonic $Ag-TiO_2$ Nanocomposites. *Nanotechnology* **2016**, *27*, 325202. [CrossRef]

78. Ambreen, J.; Haleem, A.; Shah, A.A.; Mushtaq, F.; Siddiq, M.; Bhatti, M.A.; Shah Bukhari, S.N.U.; Chandio, A.D.; Mahdi, W.A.; Alshehri, S. Facile Synthesis and Fabrication of NIPAM-Based Cryogels for Environmental Remediation. *Gels* **2023**, *9*, 64. [CrossRef]

79. Kumar Inwati, G.; Kumar, P.; Roos, W.D.; Swart, H.C. Thermally Induced Structural Metamorphosis of ZnO:Rb Nanostructures for Antibacterial Impacts. *Colloids Surf. B Biointerfaces* **2020**, *188*, 110821. [CrossRef]

80. Singh, C.; Mehata, A.K.; Priya, V.; Malik, A.K.; Setia, A.; Suseela, M.N.L.; Vikas, M.N.L.; Gokul, P.; Samridhi, P.; Singh, S.K.; et al. Bimetallic Au–Ag Nanoparticles: Advanced Nanotechnology for Tackling Antimicrobial Resistance. *Molecules* **2022**, *27*, 7059. [CrossRef]

81. Khan, S.; Iqbal, T.; Ahmed, N.; Jamil, A. Antioxidant, hemolytic and mutagenic potential of *Psoralea corylifolia*. *J. Anim. Plant Sci.* **2015**, *25*, 1451–1456.

82. Zia udDen, N.; Shahid, M. Determination of Bioactive Properties of Different Temperature *Camellia Sinensis* (Green Tea). *Am. J. Food Nutr.* **2017**, *5*, 10–18.

83. Zuber, M.; Tabasum, S.; Jamil, T.; Shahid, M.; Hussain, R.; Feras, K.S.; Bhatti, K.P. Biocompatibility and Microscopic Evaluation of Polyurethane-Poly(Methyl Methacrylate)-Titnanium Dioxide Based Composites for Dental Applications. *J. Appl. Polym. Sci.* **2014**, *131*, 39806. [CrossRef]

84. Phong, L.T.H.; Manh, D.H.; Nam, P.H.; Lam, V.D.; Khuyen, B.X.; Tung, B.S.; Bach, T.N.; Tung, D.K.; Phuc, N.X.; Hung, T.V.; et al. Structural, Magnetic and Hyperthermia Properties and Their Correlation in Cobalt-Doped Magnetite Nanoparticles. *RSC Adv.* **2021**, *12*, 698–707. [CrossRef]

85. Ramana, P.V.; Rao, K.S.; Kumar, K.R.; Kapusetti, G.; Choppadandi, M.; Kiran, J.N.; Rao, K.H. A Study of Uncoated and Coated Nickel-Zinc Ferrite Nanoparticles for Magnetic Hyperthermia. *Mater. Chem. Phys.* **2021**, *266*, 124546. [CrossRef]

86. Talaei, M.; Hassanzadeh-Tabrizi, S.A.; Saffar-Teluri, A. Synthesis of Mesoporous $CuFe_2O_4@SiO_2$ Core-Shell Nanocomposite for Simultaneous Drug Release and Hyperthermia Applications. *Ceram. Int.* **2021**, *47*, 30287–30297. [CrossRef]

87. Oh, Y.; Lee, N.; Kang, H.W.; Oh, J. In Vitro Study on Apoptotic Cell Death by Effective Magnetic Hyperthermia with Chitosan-Coated $MnFe_2O_4$. *Nanotechnology* **2016**, *27*, 115101. [CrossRef]

88. Kalita, V.M.; Tovstolytkin, A.I.; Ryabchenko, S.M.; Yelenich, O.V.; Solopan, S.O.; Belous, A.G. Mechanisms of AC Losses in Magnetic Fluids Based on Substituted Manganites. *Phys. Chem. Chem. Phys.* **2015**, *17*, 18087–18097. [CrossRef]

89. Angelakeris, M. Magnetic Nanoparticles: A Multifunctional Vehicle for Modern Theranostics. *Biochim. Biophys. Acta-Gen. Subj.* **2017**, *1861*, 1642–1651. [CrossRef]

90. Jadhav, S.V.; Kim, B.M.; Lee, H.Y.; Im, I.C.; Rokade, A.A.; Park, S.S.; Patil, M.P.; Kim, G.D.; Yu, Y.S.; Lee, S.H. Induction Heating and in Vitro Cytotoxicity Studies of $MnZnFe_2O_4$ Nanoparticles for Self-Controlled Magnetic Particle Hyperthermia. *J. Alloys Compd.* **2018**, *745*, 282–291. [CrossRef]

91. Hemery, G.; Garanger, E.; Lecommandoux, S.; Wong, A.D.; Gillies, E.R.; Pedrono, B.; Bayle, T.; Jacob, D.; Sandre, O. Thermosensitive Polymer-Grafted Iron Oxide Nanoparticles Studied by in Situ Dynamic Light Backscattering under Magnetic Hyperthermia. *J. Phys. D. Appl. Phys.* **2015**, *48*, 494001. [CrossRef]

92. Li, Z.; Kawashita, M.; Araki, N.; Mitsumori, M.; Hiraoka, M.; Doi, M. Magnetite Nanoparticles with High Heating Efficiencies for Application in the Hyperthermia of Cancer. *Mater. Sci. Eng. C* **2010**, *30*, 990–996. [CrossRef]

93. Dennis, C.L.; Jackson, A.J.; Borchers, J.A.; Hoopes, P.J.; Strawbridge, R.; Foreman, A.R.; Van Lierop, J.; Grüttner, C.; Ivkov, R. Nearly Complete Regression of Tumors via Collective Behavior of Magnetic Nanoparticles in Hyperthermia. *Nanotechnology* **2009**, *20*, 395103. [CrossRef]

94. Mehdaoui, B.; Meffre, A.; Lacroix, L.M.; Carrey, J.; Lachaize, S.; Gougeon, M.; Respaud, M.; Chaudret, B. Large Specific Absorption Rates in the Magnetic Hyperthermia Properties of Metallic Iron Nanocubes. *J. Magn. Magn. Mater.* **2010**, *322*, L49–L52. [CrossRef]
95. Pradhan, P.; Giri, J.; Samanta, G.; Sarma, H.D.; Mishra, K.P.; Bellare, J.; Banerjee, R.; Bahadur, D. Comparative Evaluation of Heating Ability and Biocompatibility of Different Ferite-Based Magnetic Fluids for Hyperthermia Application. *J. Biomed. Mater. Res.-Part B Appl. Biomater.* **2007**, *81*, 12–22. [CrossRef]
96. Dennis, C.L.; Jackson, A.J.; Borchers, J.A.; Ivkov, R.; Foreman, A.R.; Lau, J.W.; Goernitz, E.; Gruettner, C. The Influence of Collective Behavior on the Magnetic and Heating Properties of Iron Oxide Nanoparticles. *J. Appl. Phys.* **2008**, *103*, 7–9. [CrossRef]